J. Math. Study
doi: 10.4208/jms.v48n2.15.05

Vol. **48**, No. 2, pp. 187-198
June 2015

An Adaptive Grid Method for a Non-Equilibrium PDE Model from Porous Media

Paul Andries Zegeling*

Department of Mathematics, Faculty of Science, Utrecht University, the Netherlands

Received 25 March, 2015; Accepted (in revised version) 22 May, 2015

Abstract. An adaptive grid method is applied to a PDE model from geo-hydrology. Due to the higher mixed-order derivative, non-monotone waves can appear which could represent similar structures as observed in laboratory experiments [5, 16, 18]. The effectiveness of the adaptive grid, which is based on a smoothed equidistribution principle, is shown compared to uniform grid simulations. On a uniform grid (numerical) oscillating non-monotone waves may appear which are not present in the adaptive grid.

AMS subject classifications: 35Mxx, 35M11, 65Mxx, 65M20, 65M50

Key words: Adaptive grids, Method of lines, Dynamical systems, Travelling waves, Monotonicity, Porous media, Water saturation.

1 Introduction

Non-monotone waves play an important role in geo-hydrology. In particular, these phenomena are observed in laboratory experiments with, so-called, saturation overshoot and fingering structures. Figure 1 shows such behaviour in two-phase porous media, similar to the solutions and structures observed in [5, 16, 18]. The left frame illustrates saturation profiles for different values of the injection rate of the water at the left boundary of the domain, starting with initially dry sand in the tube. This corresponds with an almost one-dimensional domain in terms of the underlying PDE model. We can see monotone waves (for low injection rates), non-monotone waves (for average injection rates) and plateau-type waves (for high injection rates). The second frame depicts fingering behaviour in a higher-dimensional setting, similar to the solutions described in [16], in which the black spots indicate the overshoots compared to the blue regions where monotone 'flat' waves exist. It is known from PDE theory that the traditional models to describe flows in porous media, such as Richards' equation or the Buckley-Leverett equation, only possess monotone waves [9, 10, 12]. To deal with this problem, Hassanizadeh and Gray [11] proposed

*Corresponding author. *Email addresses:* P.A.Zegeling@uu.nl (P.-A. Zegeling)

a PDE model, using a thermodynamics approach, with an additional term in the model to include non-static conditions for the capillary pressure. Such a model which includes a mixed higher-order term, gives rise to travelling waves (TWs) with non-monotone profiles. This behaviour can be explained using an analysis from dynamical systems theory in which stationary points in the phase plane are connected by a special curve, called the separatrix. To support the theoretical considerations, numerical experiments for the PDE model are performed. For an accurate treatment of the numerical PDE solution, it is of importance to approximate the steep waves by an adaptive grid method. To my knowledge, no adaptive methods have been applied yet to this non-equilibrium PDE model. Only a few articles in literature deal with adaptive methods applied to porous media (either for the traditional theory with monotone waves or for other theoretical models with non-monotone waves): [7,8,13]. For an efficient application of adaptive grid methods, it is known from literature ([1,3,4,14,15,19–21]) that smoothness of the non-uniform grid in the space- and time-direction is crucial. Therefore, the adaptive grid method in this paper is enhanced with smoothing operators both in space and time.

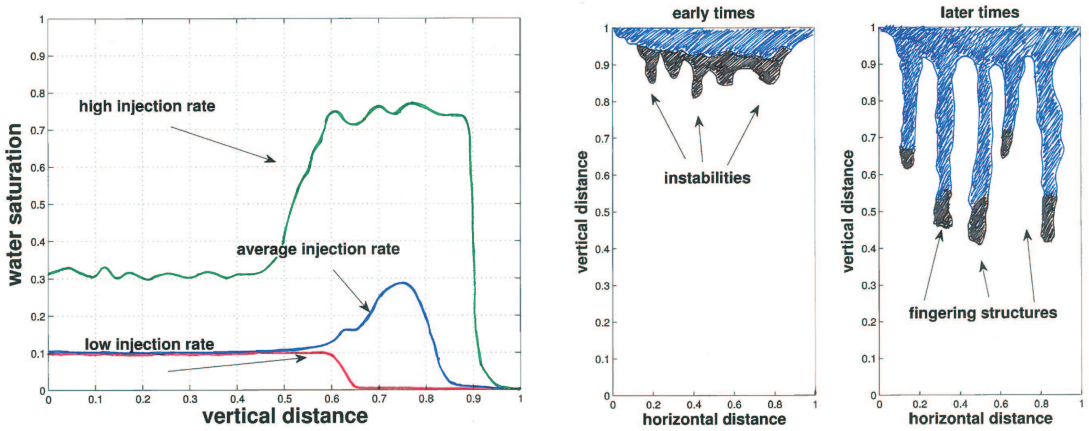

Figure 1: A sketch of two different types of laboratory experiments with non-monotone waves and fingering behaviour (left frame: monotone, non-monotone and plateau waves, similar to the ones observed in [5,18] and right frame: the occurence of instabilities and fingering behaviour, similar to the observations in [16]).

The paper is organized as follows. Section 2 introduces the non-equilibrium PDE, the so-called τ-model. Section 3 discusses the existence of travelling waves in the PDE and its dependence on the non-equilibrium parameter τ. In Section 4 we work out the adaptive moving grid method in terms of a coordinate transformation. The numerical results showing the different scenarios are described in Section 5. The main features of the model are described by three important cases, which also can be found in the second frame of Figure 1: monotone waves, non-monotone waves with oscillations and non-monotone waves with the formation of plateaus. The appearance of each of these waves depends strongly on the parameters in the model. Finally, Section 6 summarizes the conclusions.

2 A higher-order non-equilibrium PDE model from porous media

In this paper we investigate a mixed higher-order PDE model from hydrology of the form:

$$\frac{\partial S}{\partial t}=\delta\,\frac{\partial^2 S}{\partial z^2}+\frac{\partial}{\partial z}[f(S)]+\tau\frac{\partial^3 S}{\partial t\partial z^2},\quad (z,t)\in[z_L,z_R]\times(0,T], \tag{2.1}$$

with initial condition $S(z,0)=S_0(z)$. The dependent variable $S(z,t)\in[0,1]$ represents water saturation, $\delta>0$ is a diffusion coefficient and $\tau\geq 0$ a non-equilibrium parameter (see [9–11]). The function f satisfies: $f(0)=0, f(1)=1, f'(S)>0$ and may be related to a so-called fractional flow function in the full porous media model [9]. In particular we distinguish between two choices for the function f. The first choice is a convex-shaped function, representing a one phase situation (water):

$$f(S)=S^2, \tag{2.2}$$

and the second choice is a convex-concave function, indicating two phases (water and air):

$$f(S)=\frac{S^2}{S^2+M(1-S)^2}. \tag{2.3}$$

We impose the Dirichlet boundary conditions: $S(z_L,t)=S_-$ and $S(z_R,t)=S_+$. The initial function $S_0(z)$, the boundaries of the spatial domain, the final time T and the values for $0\leq S_-<S_+\leq 1$, δ and τ will be specified in the numerical results section. The parameter $M\geq 1$ in (2.3) is related to the ratio between water viscosity and air viscosity. In our experiments we set the parameter M equal to 1. For the full PDE model (not treated in this paper) including, among others, the effect of gravity and nonlinear diffusion, other values of M have to be chosen.

3 Non-monotone travelling waves

In this section we describe special types of solutions in PDE model (2.1). Especially, we are interested in so-called travelling wave (TW) solutions. For simplicity, we assume now that $f(S)=S^2$. The convex-concave case (2.3) is treated in [9, 10] which gives rise to an even richer structure of the dynamics. The TW Ansatz, assuming a positive constant speed c, is defined by:

$$S(z,t)=\phi(z+c\,t)=\phi(\eta),\ \eta\in(-\infty,+\infty),\ c>0.$$

Substituting this in PDE (2.1), we arive at the third-order ODE:

$$c\,\phi'=\delta\,\phi''+[f(\phi)]'+c\,\tau\,\phi''', \tag{3.1}$$

where the $'$ denotes taking derivatives with respect to the TW-variable η. Integrating (3.1) once between $-\infty$ and η and using the fact that $\phi(-\infty)=S_-$, $\phi'(-\infty)=\phi''(-\infty)=0$, gives the second-order ODE:

$$c\ (\phi-S_-)=\delta\ \phi'+f(\phi)-f(S_-)+c\ \tau\ \phi''. \tag{3.2}$$

To obtain an asymptotic expression for the wave speed c, we can take the limit $\eta\to\infty$ and use the fact that $\phi(+\infty)=S_+$, $\phi'(+\infty)=\phi''(+\infty)=0$. This yields (asymptotically):

$$c=\frac{f(S_+)-f(S_-)}{S_+-S_-}=\frac{S_++S_-}{2}\quad\text{(for the convex case).} \tag{3.3}$$

For the analysis of the TW solutions, it is useful to re-write ODE (3.2) as a Liénard-type system of ODEs:

$$\begin{cases}\phi'=\psi\\ c\ \tau\ \psi'=c(\phi-S_-)+f(S_-)-f(\phi)-\delta\ \psi.\end{cases} \tag{3.4}$$

A TW for (2.1) in the original coordinate system (x,t) is a specific trajectory (the "separatrix") in the (ϕ,ψ)-plane (the phase plane) connecting an unstable critical point (at $\eta=-\infty$) of ODE system (3.4) with a stable one (at $\eta=+\infty$). There are only two critical points in system (3.4):

$$(\phi,\psi)=(S_-,0),\quad\text{and}\quad(\phi,\psi)=(S_+,0).$$

From the eigenvalues of the linearized system of (3.4) we can determine the character of each of the two points. The eigenvalues can easily be calculated:

$$\lambda_\pm=\frac{-\delta}{2\tau c}\pm\sqrt{D},\ \text{with}\ D=\frac{\delta^2}{4\tau^2c^2}+\frac{S_+-S_-}{2\tau c}. \tag{3.5}$$

From (3.5) it follows that the point $(S_-,0)$ is an (unstable) saddle point in all possible cases, since $\lambda_+\lambda_-<0$. Depending on the PDE parameters δ and τ we distinguish between the following two cases for the other critical point $(S_+,0)$:

- I. a stable focus (spiral point), if $D<0$,;
- II. a stable node, if $D\geq 0$.

Non-monotone TWs exist for $\tau>\tau_{crit}=\frac{\delta^2}{S_+-S_-}$ since the saddle point is then connected to a spiral point. In Figure 2 this situation is clarified in terms of a bifurcation diagram (left panel) and a phase plane plot (right panel). For $\tau=0$, i.e. the model is a Burgers' (for f as in (2.2)) or Buckley-Leverett equation (for f as in (2.3)), it is known that only monotone waves satisfy the PDE model [2]. The blue vertical line for $\tau=0$ describes the case of a viscous Burgers' equation, whereas the red dot with $\tau=\delta=0$ indicates the inviscid Burgers' equation with possible shock solutions. For $\delta=0$ and $\tau>0$ (the blue horizontal line with marks) no TW solutions exist. Since we are looking also for 'fingering' structures

or, at least, non-monotone waves, we need the extra τ-term in PDE (2.1) to describe such phenomena. Note again that the convex-concave case (2.3) is treated in [9]. There, in addition, plateau-type waves may appear. In that case three critical points exist in the dynamical system with a much more complicated behaviour in the phase plane. We will find these plateau-waves in the numerical solutions in the next section by using an adaptive grid method to solve the PDE model (2.1).

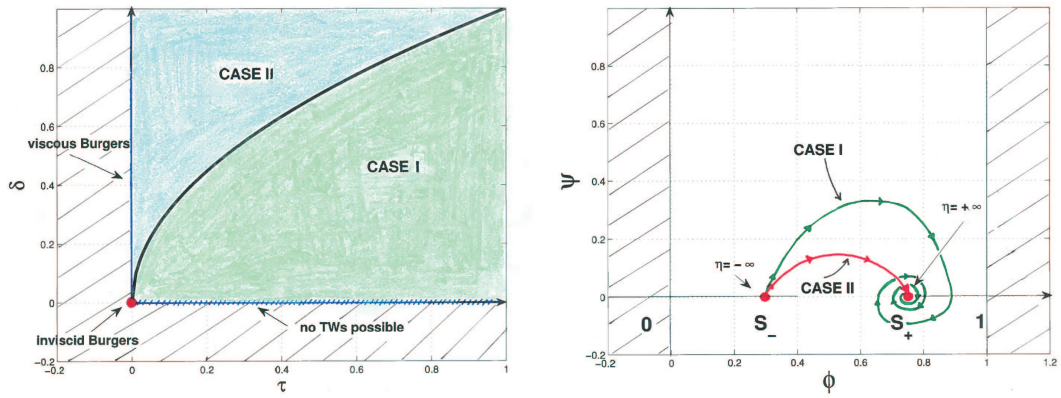

Figure 2: A bifurcation diagram (left) indicating the existence of monotone-(Case II) and non-monotone (Case I) waves depending on the parameters δ and τ. The black curve is defined by: $\delta=\sqrt{\tau(S_+-S_-)}$. The right plot shows, for two different values of the parameter τ, trajectories in the phase plane (ϕ,ψ). The green curve corresponds to a non-monotone wave ($\tau>\tau_{crit}>0$, Case I) and the red curve denotes a monotone wave ($\tau=0$, Case II).

4 The adaptive moving grid method

For the efficient and accurate numerical computation of the travelling waves appearing in PDE model (2.1), we employ an adaptive grid method that has shown its usefullness in many other cases, see for example [6, 20]. The idea behind the adaptive grid method, which is based on a fixed number of spatial grid points ('r-refinement'), is to first transform the PDE using another general coordinate system (see Figure 3). The second step is to define the adaptive transformation and to discretize the coupled system of two PDEs in the spatial direction. In the final step, an implicit time-integration method is applied to the semi-discrete ODE system to give the full numerical solution at all space and time grid points.

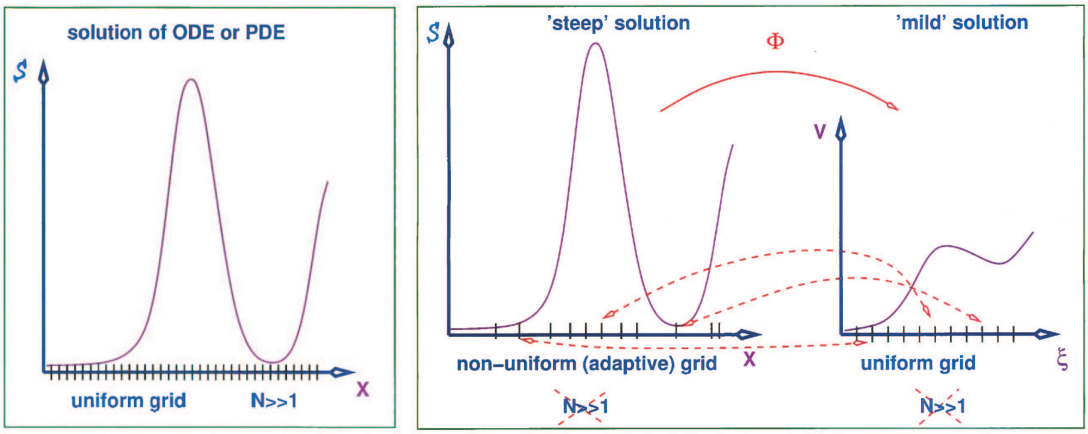

Figure 3: An explanation of the use of the adaptive transformation Φ (right panel): the goal is to transform the 'steep' dependent variable S into a 'milder' variable v in the new coordinates such that a fewer number of spatial grid points N (right panel) is needed compared to the uniform grid case with $N \gg 1$ in the left panel (for a comparable accuracy).

4.1 Transforming the PDE model

The general coordinate transformation is given by

$$\begin{cases} z = z(\zeta,\theta), \\ t = t(\zeta,\theta) = \theta. \end{cases} \tag{4.1}$$

The determinant of the Jacobian of (4.1) can be worked out to get: $\mathcal{J} := \frac{\partial z}{\partial \zeta}$ (shorter notation: z_ζ) and with $v(\zeta,\theta) := S(z(\zeta,\theta),\theta)$, we obtain the PDE in the new coordinates:

$$\mathcal{J} v_\theta - (v + z_\theta) v_\zeta = \delta \left(\frac{v_\zeta}{\mathcal{J}}\right)_\zeta + \tau \left[\mathcal{J}\left(\frac{1}{\mathcal{J}}\left(\frac{v_\zeta}{\mathcal{J}}\right)_\zeta\right)_\theta - z_\theta\left(\frac{1}{\mathcal{J}}\left(\frac{v_\zeta}{\mathcal{J}}\right)_\zeta\right)_\zeta\right]. \tag{4.2}$$

The idea is to couple PDE (4.2) to an adaptive grid PDE which defines the transformation implicitly and completes the system of equations. In the new coordinates then a basic uniform grid (second-order) discretization is used in the ζ-direction ($\Delta\zeta$ is constant). This gives a strongly coupled nonlinear and stiff ordinary differential equation system, for which an appropriate time-integration technique must be used to obtain the final numerical solution at each gridpoint in time and space.

4.2 Equidistribution with smoothing

We apply an adaptive grid in terms of the coordinate transformation which satisfies the fourth-order (in space) and first-order (in time) PDE [14,20,21]:

$$\left[\left(\mathcal{S}(\mathcal{J}) + \tau_s \mathcal{J}_\theta\right) \omega\right]_\zeta = 0, \quad \tau_s \geq 0.$$

Here,

$$\omega := \sqrt{1+(\frac{v_\zeta}{\mathcal{J}})^2} = \sqrt{1+(S_z)^2}$$

is a so-called monitor function, reflecting the dependence of the non-uniform grid on the first-order spatial derivative: $S_z = \frac{v_\zeta}{\mathcal{J}} = \frac{v_\zeta}{z_\zeta}$. The operator

$$\mathcal{S} := \mathcal{I} + \sigma_s(\sigma_s+1)\frac{\partial^2}{\partial\zeta^2}$$

is used to obtain a smoother grid transformation in space. Here, $\sigma_s > 0$ is a spatial smoothing (or filtering) parameter. Finally, the parameter τ_s takes care of the smoothness in the time-direction.
For $\sigma_s = \tau_s = 0$ (no smoothing), we return to the basic equidistribution principle $(z_\zeta \omega)_\zeta = 0$, which is a continuous representation of the discrete equidistribution property:

$$\Delta z_i \; \omega_i = constant.$$

This property indicates that the grid will be concentrated (Δz_i small) in areas of high spatial activity for which ω_i is large (keeping their product constant). However, without additional smoothing, the numerical calculation of the combined grid PDE and physical PDE is likely to give irregular grid distributions and, therefore, creates difficulties for the numerical time-integrator. For $\sigma_s > 0$ and $\tau_s > 0$, after discretization, it can be shown [14] that the spatial grid will satisfy a local-quasi uniformity condition

$$\frac{\sigma_s}{\sigma_s+1} \leq \frac{\Delta z_{i+1}}{\Delta z_i} \leq \frac{\sigma_s+1}{\sigma_s}$$

for all gridpoints z_i. The combination of both smoothing operators produces both smoothly distributed spatial grids and smooth grid trajectories in the time-direction from which the time-integration will benefit. In practice, the choice for the temporal smoothing parameter depends on the time-scales in the model: $\tau_s \approx 10^{-3}\times$ the 'critical time scale' in the PDE model, which in our situation will be $\mathcal{O}(1)$. The spatial smoothing parameter σ_s can be taken $\mathcal{O}(1)$. For more details on the adaptive grid and the smoothing operators we refer to [14, 20, 21]. The transformed PDE and the adaptive grid PDE are simultaneously semi-discretized in the spatial direction following a method-of-lines approach. The time-integration of the resulting coupled ODE-system is done by a variable fifth-order BDF method in DASSL [17].

5 Numerical experiments

In this section we give several numerical examples to show the behaviour of both the adaptive grid and the solutions in the model depending on the model parameter τ and the flux function f. The adaptive grid parameters are fixed throughout the experiments

unless otherwise specified: $\sigma_s = 2$ and $\tau_s = 0.001$. For the time-integration a tolerance in DASSL of 10^{-4} is chosen. The initial condition is a steep wave starting at the right boundary of the domain and reads:

$$S(z,0) = S_0(z) = S_- + \frac{1}{2}(S_+ - S_-)(1+\tanh(R(z-z_0)).$$

The following values for the parameters are chosen: z_L=0, z_R=1.4, S_-=0, S_+=0.6, R=50. In Figure 4 the effect of changing the smoothness parameters is displayed. Low values of the smoothing parameters cause irregular grid trajectories in time and space, whereas too high values will have a damping effect on the grid. This will lead to a slow-down of the grid motion with negative effects on the accuracy. Figure 5 shows the convergence of both the uniform and adaptive method with an increasing number of spatial grid points, keeping the same time-tolerance. For the right plot, the parameters are chosen such that $\tau > \tau_{crit}$. Note that the adaptive grid needs approximately a factor of four fewer gridpoints than the uniform grid method (for the same accuracy). In Figure 6 we see that unnatural oscillations on a uniform grid may show up (left panels), when the solution should stay monotone (right panels: the adaptive grid solution). For $\tau > \tau_{crit}$ the solution itself should be non-monotone. It is, therefore, difficult to detect this difference on a uniform grid. In Figure 7 three cases are depicted on an adaptive grid with 101 grid points. In the upper three plots $\tau = 0$ (a monotone wave), $\tau = 10^{-4}$ with a convex f (non-monotone wave) in the middle three plots and in the lower three plots with a convex-concave f (a non-monotone wave with a plateau-shape). These waves are predicted by the analysis in Section 3 and [9].

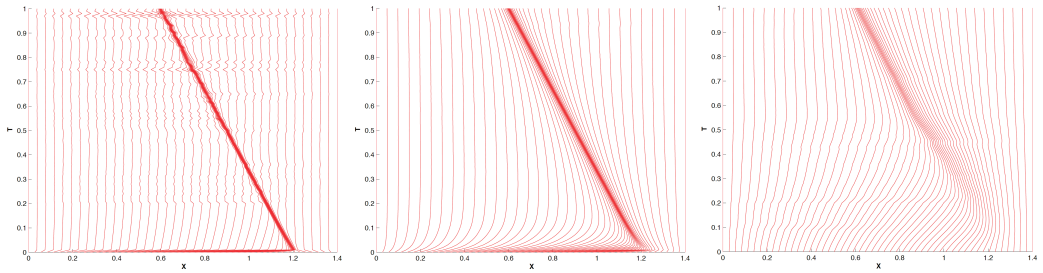

Figure 4: Time history of an adaptive grid without spatial smoothing (left), i.e. with $\sigma_s = 0$, a grid with smoothing in both independent variables (middle) and a grid with too much smoothing, $\tau_s = 0.3$ (right).

6 Conclusions

Travelling wave solutions for a non-equilibrium PDE model from hydrology are analyzed and numerically approximated. Depending on the non-equilibrium parameter $\tau \geq 0$ both monotone and non-monotone waves can be predicted analytically. For the efficient and accurate numerical approximation of such waves, smooth adaptive grids in space and

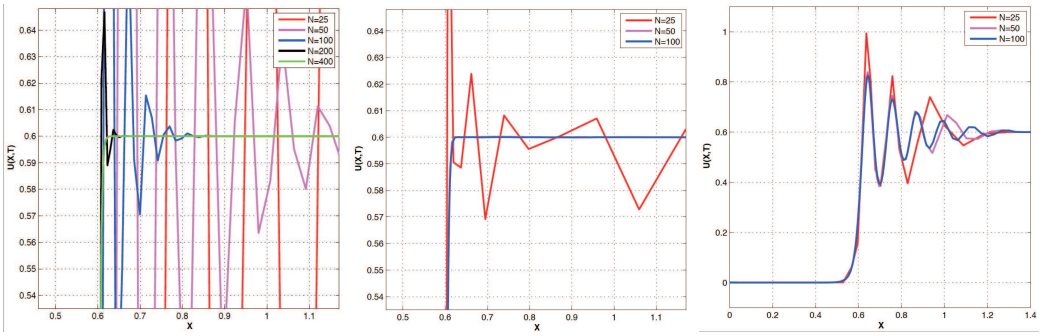

Figure 5: Convergence of uniform and adaptive grid solutions for increasing values of N, $\tau=0$ (left two plots: uniform grid vs adaptive grid) and $\tau>0$ with a convex function f (right plot). The number of grid points is increased from $N=25$ to 400 by doubling in the left frame and from $N=25$ to 100 in the adaptive case (central plot). The right plot indicates the convergence of the adaptive method for the case $\tau=3\times10^{-4}$, $\delta=2\times10^{-3}$ for the convex fractional flow function f.

time are used. Since the model possesses an extra mixed higher-order derivative term, special attention has to be paid to the adaptive grid transformation of the PDE model. When uniform grids are being used, non-monotone waves can even appear in situations for which monotonicity is predicted theoretically. The adaptive grid method needs, in the experiments as described in this paper, approximately a factor 4 fewer grid points than the uniform grid case (for obtaining the same accuracy). This factor will be higher for cases with smaller diffusion coefficients δ. The dependence of this gain factor on the parameter τ is unclear. The effect of high values of τ has still to be investigated. Additionally, one should mention that application of the adaptive grid requires the solution of an extra nonlinear grid PDE combined with the transformed original physical PDE model. The numerical solution of the combined nonlinear system of equations, yields, of course, some loss of efficiency. In an earlier paper (see [20]) we have investigated the efficiency of the current adaptive grid approach.

References

[1] C. Budd, W. Huang and R. Russell. Adaptivity with moving grids. Acta Numerica, 1-131, 2009.

[2] C. Cuesta, C. J. van Duijn and J. Hulshof. Infiltration in porous media with dynamic capillary pressure: travelling waves. Eur. J. Appl. Math, 11, 381-397, 2000.

[3] A. van Dam and P. A. Zegeling. A robust moving mesh finite volume method applied to 1d hyperbolic conservation laws from magnetohydrodynamics. J. of Comput. Phys. 216: 526-546, 2006.

[4] A. van Dam and P. A. Zegeling. Balanced monitoring of flow phenomena in moving mesh methods. Commun. Comput. Phys. 7: 138-170, 2010 .

[5] D. DiCarlo. Experimental measurements of saturation overshoot on infiltration. Water Resources Research, V40, W04215, 2004.

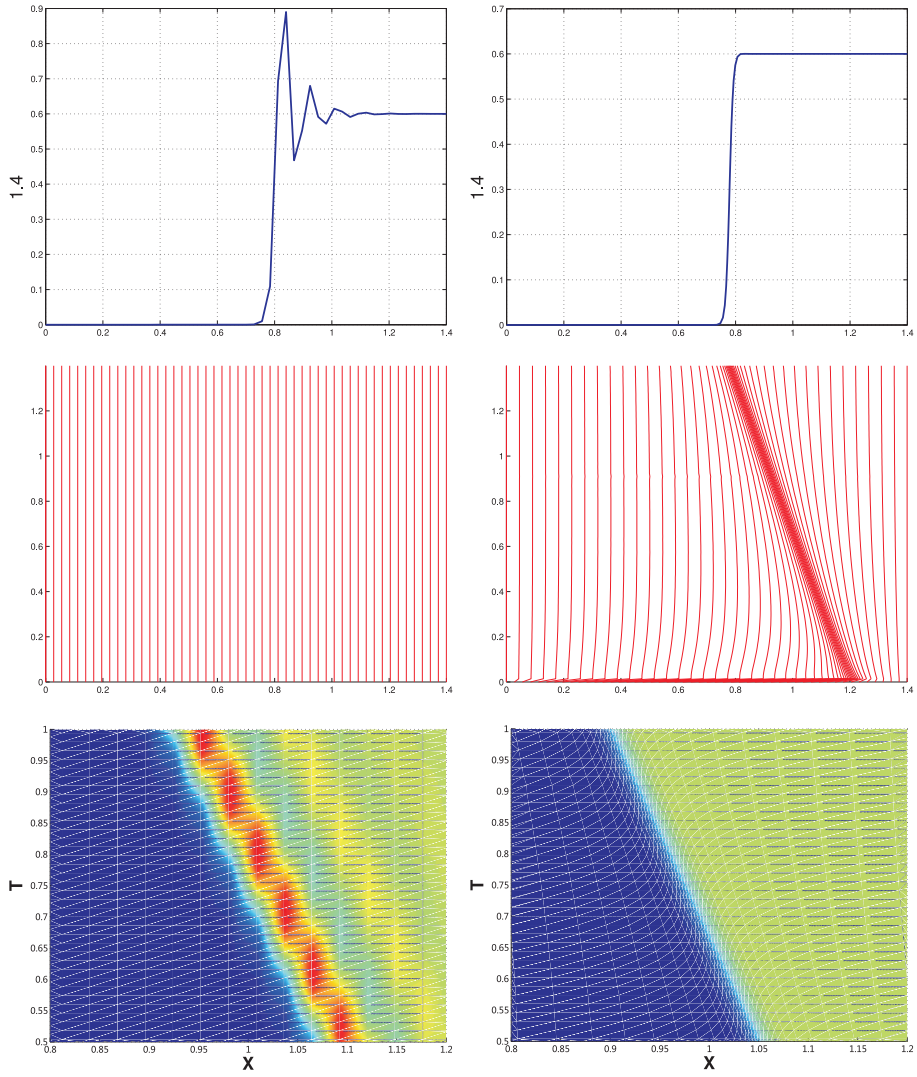

Figure 6: Comparison of adaptive (right three pilots) and uniform grid (left three plots) calculations for $N=101$ and $\tau=0$ (monotone solutions of the PDE model). The two top frames show the numerical solution at $t=1.4$, the middel two frames show the grid behaviour in time, and the lower two frames give a close-up of the solution pattern between $t=0.5$ and $t=1$. We observe numerical oscillations on the uniform grid, clearly indicating the irregularities in the numerical solution. The adaptive grid follows the steep wave with the correct constant velocity $c=0.3$ (see also equation (3.3)).

[6] A. Doelman, T. Kaper and P. A. Zegeling. Pattern formation in the 1-D Gray-Scott model. Nonlinearity, 10: 523-563, 1997.

[7] H. Dong, Z. Qiao, S. Sun and T. Tang. Adaptive grid methods for two-phase flow in porous media. J. of Comp. and Appl. Maths., 265, 2014.

[8] F. Doster, P. A. Zegeling and R. Hilfer. Numerical solution of a generalized theory for macroscopic capillarity, Physical Review, E81, 036307, 2010.

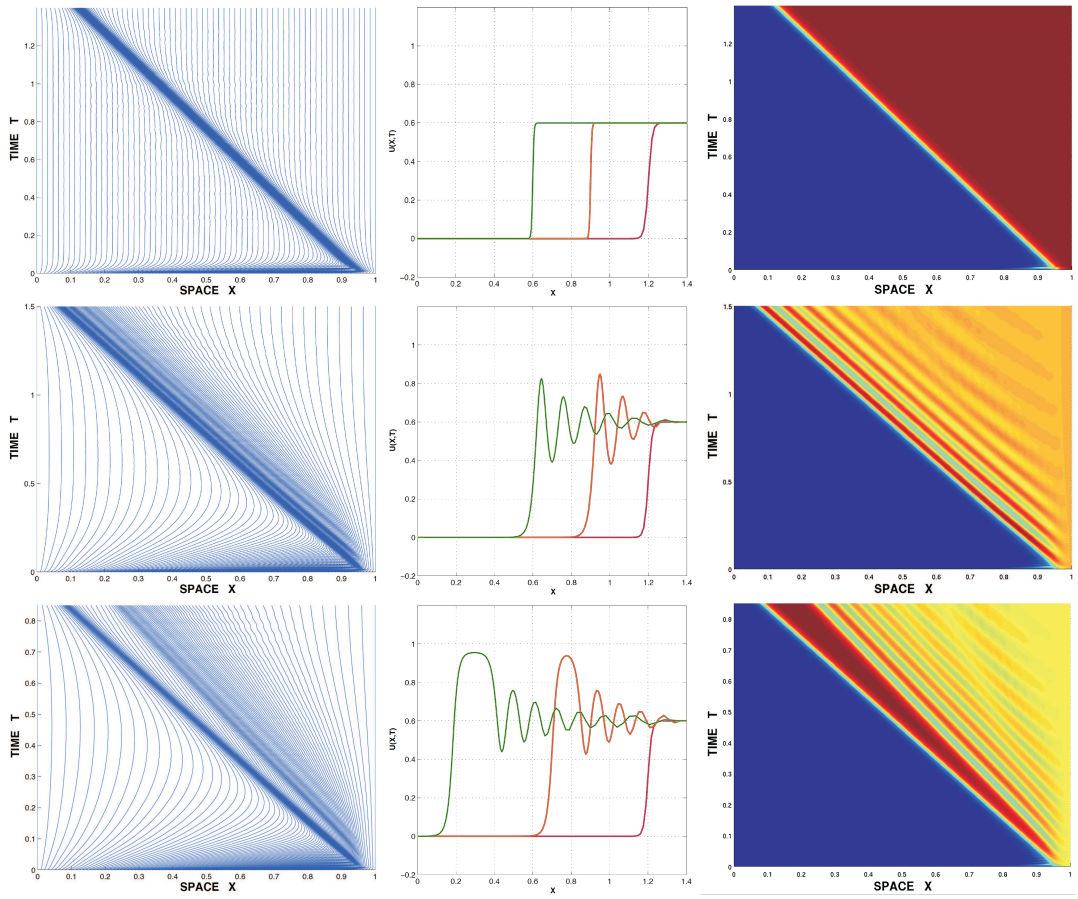

Figure 7: The time history of the adaptive grid (left), the solutions at three points of time (center) and pattern plots (right) for three characteristic cases in the porous media model: $\tau=0$ (top), $\tau=10^{-4}$ with a convex f (middle) and with a convex-concave f (bottom).

[9] C. J. van Duijn, Y. Fan, L. A. Peletier and I. S. Pop. Travelling wave solutions for a degenerate pseudo-parabolic equation modelling two-phase flow in porous media. Nonlinear Anal. Real World Appl, 1361-1383, 2013.

[10] C. J. van Duijn, S. M. Hassanizadeh, I. S. Pop and P.A. Zegeling. Non-equilibrium models for two-phase flow in porous media: the occurence of saturation overshoot. Proc. of the Fifth Int. Conf. on Appl. of Porous Media, Cluj-Napoca, 2013.

[11] S. M. Hassanizadeh and W. G. Gray. Thermodynamic basis of capillary pressure on porous media, Water Resources Research. 29: 3389-3405, 1993.

[12] R. Hilfer, F. Doster and P. A. Zegeling. Nonmonotone saturation profiles for hydrostatic equilibrium in homogeneous porous media, Vadose Zone Journal, V11, N3, 201, 2012.

[13] G. Hu and P. A. Zegeling. Simulating finger phenomena in porous media with a moving finite element method. J. of Comp. Phys., YJCPH 3432, 2011.

[14] W. Huang and R. D. Russell. Analysis of moving mesh partial differential equations with spatial smoothing. SIAM J. Num. Anal., 34: 1106-1126, 1997.

[15] W. Huang and R. D. Russell. Adaptive moving mesh methods, Springer, New York, XVII, 432p, 2011.
[16] M. J. Nicholl and R. J. Glass. Infiltration into an analog fracture: experimental observations of gravity-driven fingering. Vadose Zone Journal, 4: 1123-1151 (2005).
[17] L. R. Petzold. A Description of DASSL: A Differential/Algebraic System Solver. In: IMACS Transactions on Scientific Computation, Eds.: R.S. Stepleman *et al.*, 65-68, 1983.
[18] S. Shiozawa and H. Fujimaki. Unexpected water content profiles under flux-limited one-dimensional downward infiltration in initially dry granular media. Water Resources Research, V40, W07404, 2004.
[19] T. Tang and H. Tang. Adaptive mesh methods for one- and two-dimensional hyperbolic conservation laws. SIAM Journal on Numerical Analysis, Volume 41 Issue 2: 487 - 515, 2003.
[20] P. A. Zegeling, I. Lagzi and F. Izsak. Transition of Liesegang precipitation systems: simulations with an adaptive grid PDE method, Communications in Computational Physics. Vol. 10, No. 4: 867-881, 2011.
[21] P. A. Zegeling. Theory and Application of Adaptive Moving Grid Methods. Chapter 7 in Adaptive Computations: Theory and Computation, Science Press, Beijing, 2007.